Contrib Mineral Petrol (1993) 114:519–532

Contributions to Mineralogy and Petrology

Low-temperature coherent exsolution in alkali feldspars from high-grade metamorphic rocks of Sri Lanka

Christos Evangelakakis[1], Herbert Kroll[1], Gerhard Voll[2], Hans-Rudolf Wenk[3], Hu Meisheng[3], and Jürgen Köpcke[4]

[1] Institut für Mineralogie, Westfälische Wilhelms-Universität, Corrensstrasse 24, D-48149 Münster, Germany
[2] Institut für Mineralogie, Universität zu Köln, Zülpicher Strasse 49, D-50674 Köln, Germany
[3] Department of Geology and Geophysics, University of California, Berkeley, CA 94720, USA
[4] Institut für Physikalische Chemie, Callinstrasse 3–3A, D-30167 Hannover, Germany

Received February 26, 1992 / Accepted April 26, 1993

Abstract. In the alkali feldspars of the amphibolite- and granulite-facies rocks of Sri Lanka, a late-stage, final exsolution event is observed which produced film lamellae and fine-scale spindles. These were investigated by optical, microprobe, single-crystal, transmission electron microscopy and atomic resolution microscopy techniques. The lamellae and spindles exsolved below the coherent solvus at temperatures as low as 300 to 350° C. Precession photographs and ARM micrographs show that the intergrowth is perfectly coherent. In sections ∥(010) the rhombic section of the Pericline twins corresponds to analbite or high albite. The albite lamellae and spindles nucleated and grew at low temperatures in a metastable disordered structural state within a tweed-orthoclase matrix and became periodically twinned analbite or high albite, which subsequently developed only a slight increase in Al, Si order. The relationship between twin periodicity and lamellar width, predicted for coherent intergrowths by Willaime and Gandais (1972), is obeyed. In Or-rich grains, in which coherent exsolution is the only exsolution event, the film lamellae tend to be restricted to the rim, the fine-scale spindles to the centre of the grains. The films nucleated heterogeneously at grain boundaries and grew towards the grain centres. Fine-scale spindles probably nucleated homogeneously in the interior part of grains. Heterogeneous nucleation and coherent growth are not mutually exclusive.

Introduction

With the increasing availability of transmission electron microscopy (TEM), studies of feldspar exsolution textures include microstructural characterizations in addition to X-ray and optical observations. Concepts of coherent nucleation and spinodal decomposition, developed by Cahn (1962, 1968), were applied to exsolution in feldspars and tested by TEM (see recent reviews by Yund 1983a, b, 1984; Parsons and Brown 1984, 1991; Smith and Brown 1988). While much research has concentrated on submicroscopic exsolution features, the coarser exsolution textures that can be observed in thin sections have attracted less attention in recent years. Relatively few papers deal with the formation of coarse antiperthites and perthites (e.g. Kay 1977; Parsons 1978; Day and Brown 1980; Speer and Ribbe 1973; Yund and Ackermand 1979; Yund et al. 1980; Büsch and Mehnert 1991). More frequently, the bulk or phase composition of coexisting feldspars is used in geothermometry (Mora and Valley 1985, and citations therein; Fuhrman and Lindsley 1988; Elkins and Grove 1990). To some degree the small interest in optically visible exsolution textures may be related to the fact that the original features acquired by solid-state diffusion are often obliterated by the interaction with a late aqueous fluid phase (Worden et al. 1990), leaving little information about the early exsolution history. In dry granulite-facies rocks, however, the original textures have often escaped such an event. We have therefore chosen to study the feldspars of the amphibolite- and granulite-facies terrain of Sri Lanka. These Precambrian rocks contain feldspars exhibiting a wide range of exsolution and transformation textures which are mostly undisturbed by fluid-rock interactions. In this paper we restrict discussion to the ubiquitous film and fine-scale spindle perthites.

We will address the following questions:

1. The exsolution mechanism of film and fine-scale spindle perthites
2. The temperature or range of temperatures of exsolution
3. The structural state during exsolution and later modifications

Structural, magmatic and metamorphic history of Sri Lanka

We first give a short account of the lithological, deformational and metamorphic history of Sri Lanka to place the feldspars in

Correspondence to: H. Kroll

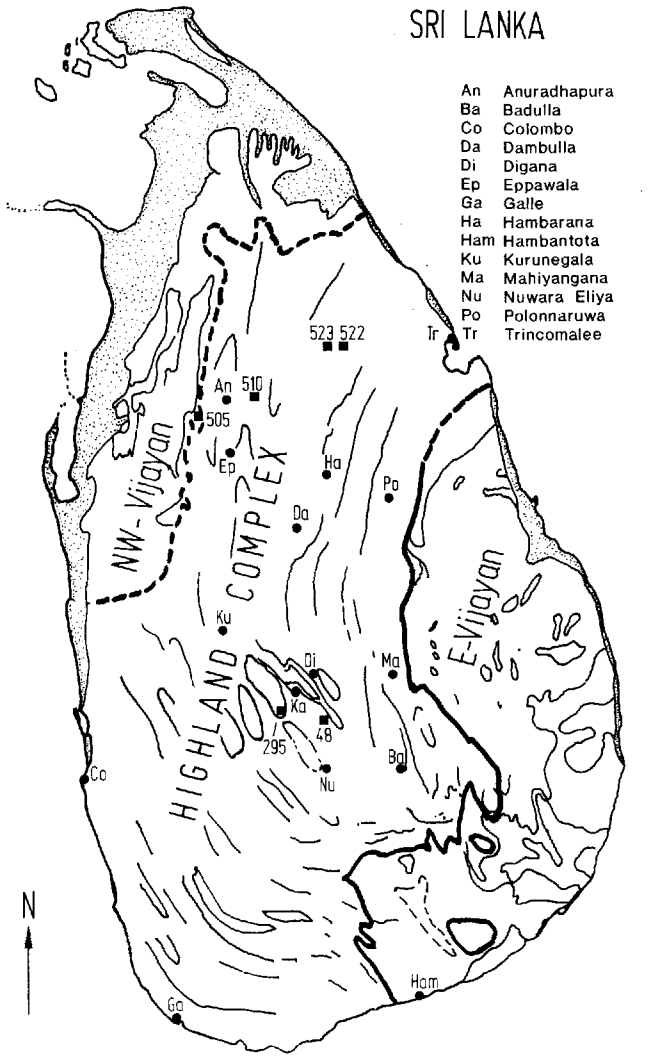

Fig. 1. Simplified geological map of Sri Lanka with major lithotectonic units. Boundaries shown are based on the geological map of Sri Lanka (1982). Numbers refer to sample numbers (e.g., *510*, VSL510 in Table 1)

a proper geological context. A more complete account, based on extensive field work, is given by Voll and Kleinschrodt (1991). The feldspar-bearing rock samples studied in this paper are described by Voll et al. (in press). The geochemistry, geothermobarometry, stable isotopes, and geochronology of the rocks were investigated by other members of a German Sri Lankan research team (Precambrian Research, Special Issue, in press). Two-feldspar geothermometry was modified by Kroll et al. (in press) to account for the effects of retrograde resetting and was applied by Voll et al. (in press) to Sri Lankan feldspars.

Three units are distinguished in the basement of Sri Lanka: (1) the Highland Complex (HC); (2) the NW-Vijayan (NWV); (3) the E-Vijayan (EV) (Fig. 1). The HC consists essentially of granulite-facies rocks. In the central part, rocks of a high-temperature amphibolite-facies level are folded down and preserved in large synforms. Both, the NWV and the EV contain rocks of high-grade amphibolite-facies, characterized by ubiquitous and extensive late partial melting, which is also common in the amphibolite-facies fillings of the synforms.

The HC consists of about 80% meta-igneous rocks, which are intercalated between metasediments [quartzites, (psammo-) pelites, dolomite and calcite marbles, calcsilicate rocks, magnetite quartzites]. Unambigous metasediments are rare in both Vijayans where rocks mostly consist of granitoid gneisses, charnockitic gneisses and migmatites.

According to Hölzl et al. (1991) the regional, granulite-facies metamorphism occurred 610–550 Ma ago. It is thus of Panafrican age. The time of peak metamorphism is estimated as 610–600 Ma. Late- to post-tectonic granites in the NWV and HC yield intrusion ages of 580–550 Ma, which is also the period of migmatization ($\approx$575 Ma). The metamorphic event occurred more or less synchronously in the HC, NWV and EV.

The NWV and the HC roughly represent a section through a tilted crust. Metamorphic conditions increase from $\approx$700° C and 3–5 kbar in the west (near Colombo) to 850–900° C and 8–10 kbar in the northern and eastern parts of the HC (Raith et al. 1991; Schenk et al. 1991; Schumacher and Faulhaber, in press). Garnet ages (Hölzl et al. 1991) and petrological results (Schumacher et al. 1990; Schenk et al. 1991) indicate that slow isobaric cooling followed the metamorphic peak (2–3° C/Ma down to 600° C, 480 Ma ago). From biotite ages it is inferred that between 600° C and 350–300° C the cooling rate increased to 10 to 25° C/Ma.

Early deformation (D_1) was acquired at conditions near the *P–T* climax of metamorphism. It includes flattening of layers (ss) and N-S stretching. The planes of flattening (s_1) and stretching (str_1) are parallel to ss. Granite sills (Older Metagranites) occur in the sediments of the HC parallel to ss. Many sills arrived laden with (K, Na)-feldspar phenocrysts, i.e. within their crystallization interval. Similar metagranites occur in the NWV and the EV. In the HC, they were dated as $\approx$1.9 Ga old, in the EV as 1.0 Ga old. Hölzl et al. (1991) interpret these ages as time of emplacement of the granitoid precursors into the surrounding sediments, i.e. the continental crust of the HC is more than 1.9 Ga old, whereas the granulite-facies metamorphic event is much younger. Numerous basic sills, some of them large layered intrusions, also intruded the sediments, and even pre-existing granite sills, parallel to ss. Granite and basic sills suffered the same strong D_1 as the sediments. The alkali feldspars are partly preserved as phenocrysts, partly recrystallized, flattened and stretched.

Second and third generation folds ($D_{2,3}$; $F_{2,3}$) also formed near peak temperature. They reach km dimensions, are strongly deformed and mostly isoclinal. While $D_{2,3}$ affected some parts of the HC, in other parts D_1 deformation continued.

Very large F_4 syn- and antiforms formed after D_1 (locally after $D_{2,3}$) in all units. The largest are found in the HC. In such synform centres amphibolite-facies rocks are preserved from erosion, together with the remainders of the large basic, layered Kandy Intrusions (Voll and Kleinschrodt 1991; Kleinschrodt et al. 1991).

In the north of the HC, D_4-folding is completed at peak temperatures. There, D_1 and D_4 deform feldspars and carbonates as homogeneous solid solutions, causing recrystallization before all unmixing. In the southern half of the HC, temperature begins to drop during D_1 and alkali feldspars and carbonates start to unmix before D_1 ceased. Continued D_1 at lower temperatures, as in the Digana Movement Zone east of Kandy (Fig. 1), causes deformation of such unmixed crystals and causes them to recrystallize, now at lower temperatures. Later and thus at even lower temperatures, the Digana Movement Zone was folded by the F_4 folds.

The eastern parts of the HC are hardly affected by D_4. There all layers dip 35° to the west and lower levels are exposed towards the east. The exposure of lower levels displays higher pressure and temperature values (Raith et al. 1991; Schenk et al. 1991). The F_4-fold level gently dips from Kandy to the west towards Colombo. Therefore the lowest pressures are found in the region round Colombo.

The HC was transported as a large nappe across at least the EV from north to south (Voll and Kleinschrodt 1991; Kleinschrodt, in press). Outliers are found resting on the EV down to the south coast. Strong D_1 within the nappe, strongly increased deformation at the nappe boundary and nappe transport are all part of the same process. The thrusting occurs relatively late and granulite-facies rocks are retrograded to amphibolite-facies at the nappe contact.

Partial melting occurred at several stages. The HC metasedi-

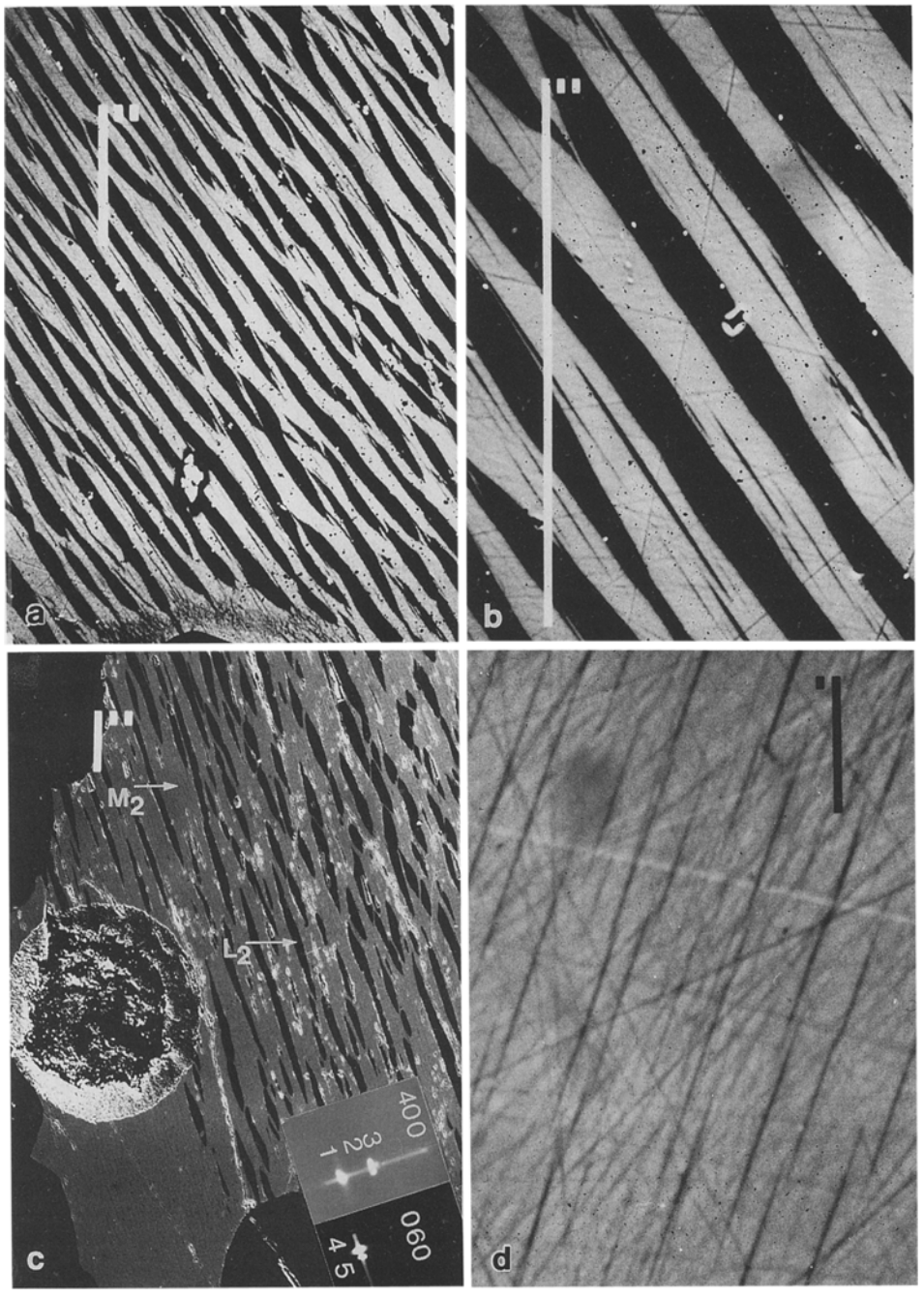

Fig. 2a–d. Electron microprobe backscatter photographs of a variety of perthites in sections $\approx \|(001)$. **a** Coarse mesoperthite with bulk composition $Or_{50.3}Ab_{44.9}An_{4.8}$ (VSL523). *Black lamellae*, Ab-rich; *white lamellae*, Or-rich. Scale bar, 100 μm. **b** Enlarged portion of Fig. 2a showing second stage Ab-rich exsolution lamellae (film albite). Scale bar, 100 μm. **c** Gradual change of the mesoperthite texture into the spindle perthite texture at $\approx Or_{60}$ in VSL295, $Or_{61.0}Ab_{38.5}An_{0.5}$. Fine-film albite occurs between coarse lamellae and lenses. Scale bar, 100 μm. *Inset*: group of 400 and 060 reflections of a precession photograph taken from the circular portion drilled out of the perthite. The single strong 400 reflection, *1*, represents the monoclinic orthoclase matrix. The poorly resolved pair of reflections, *2*, represents coarse spindles (low albite with $\gamma^* \approx 90°$) with balanced albite twinning, non-coherently intergrown with the matrix. The single weak reflection, *3*, represents coherently intergrown film albite. **d** Enlarged portion of the area to the *right* of the circular crater in Fig. 2c showing film lamellae, oriented NNE-SSW. Other lines are scratches.

ments were migmatized late during D_1. Late melting was widespread in biotite-rich rocks of higher levels, i.e. in big synforms and round Colombo. It is maximal in both Vijayans.

Rocks of all units suffered static annealing during long-lasting cooling and uplift. In the north of the HC it starts at peak temperatures surviving all deformation, in the south at temperatures of a lower granulite or an amphibolite-facies.

Nomenclature of exsolution textures

Mesoperthites ($\approx Or_{20}$ to Or_{55}) consist of intimately intergrown Ab- and Or-rich lamellae. Their interface is oriented about parallel to $(\bar{6}01)$. The lamellae do not display a host-guest relationship (Fig. 2a, b). In more Or-rich alkali feldspars the Ab-rich lamellae occur as isolated lenses and blebs in an Or-rich matrix. They tend

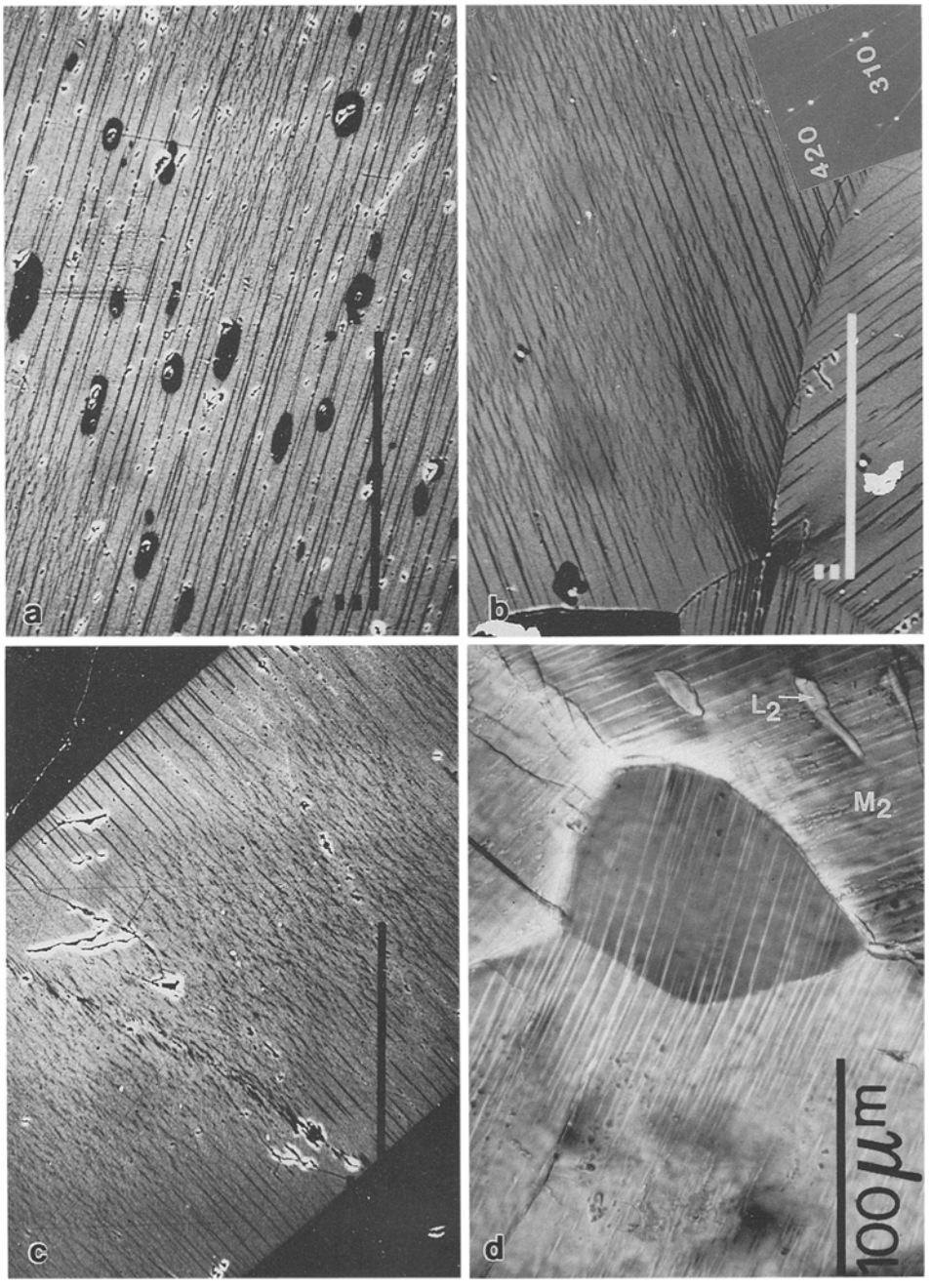

Fig. 3a–d. Electron microprobe backscatter photographs and microphotograph of a variety of perthites in sections $\approx \parallel(001)$. **a** Relatively Or-rich perthite (VSL510, $Or_{76.8}Ab_{20.3}An_{2.4}Cn_{0.5}$). Abundant coherent films and fine-scale spindles (*lower left corner* and *upper middle*) occur between rare separate non-coherently intergrown, *black*, blebs in an Or-rich matrix. Scale bar: 100 µm. **b** Three film perthite grains intersect at a triple point (VSL48–2, $Or_{80.0}Ab_{18.3}An_{0.6}Cn_{1.1}$). As seen from the thin section (Fig. 3d), these grains as well as others grew from unmixed and subsequently deformed parent grains by recrystallization. At bulk compositions $>Or_{80}$ only coherent films and fine-scale spindles are exsolved. The films are restricted to the rims where they nucleated heterogeneously at the grain boundaries. The fine-scale spindles probably nucleated homogeneously in the centre of the grains. *Inset*: part of an a^*b^* precession photograph demonstrating coherency between the films/spindles and the matrix (compare Yund 1983, Fig. 9). Scale bar, 100 µm. **c** Alkali feldspar grain (VSL1422, $Or_{81.2}Ab_{17.1}An_{0.6}Cn_{1.1}$) occurring in a plagioclase (probably not antiperthitic). Similar exsolution features as in Fig. 3b. Between coarser film lamellae apparently a second generation of fine, short lamellae has nucleated. **d** Photomicrograph: small portion of a deformed spindle perthite, VSL48-1 (*upper right corner*), and three film perthites, VSL48-2, that originated from a deformed spindle perthite by recrystallization. The non-parallel orientation of spindles and films follows from the re-orientation of the spindles caused by deformation. Deformation occurred after the spindles had exsolved and before the films unmixed. If the crystallographic orientation of two adjacent grains is similar, films nucleating in the common grain boundary grow sideways into both grains

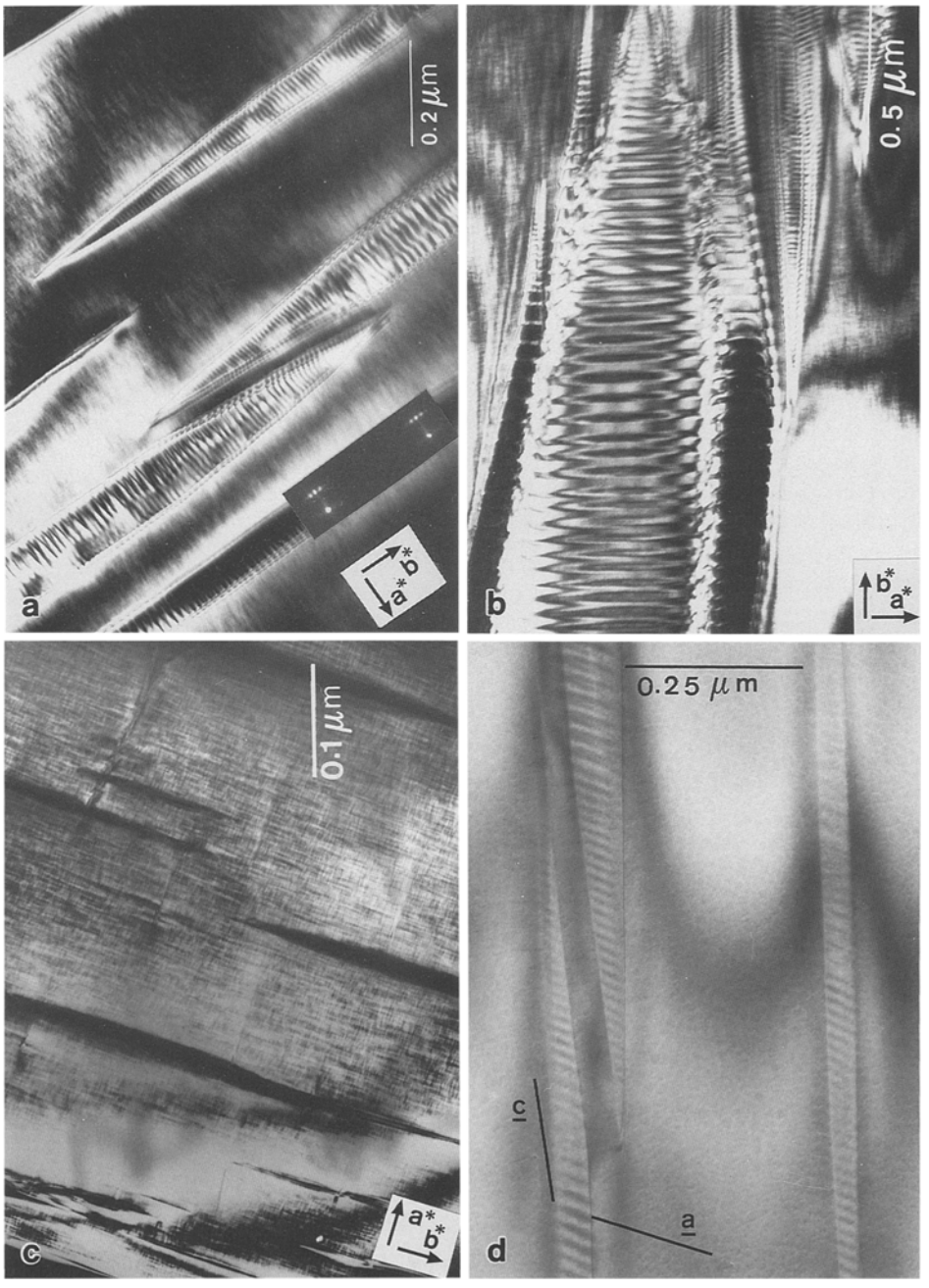

Fig. 4a–d. Dark-field electron micrographs of film lamellae. **a, b** Film lamellae with periodic Albite twinning. Note that the twin periodicity varies with lamellar width (**a** VSL49, **b** VSL510). The films are embedded in a tweed-orthoclase matrix. Electron beam parallel to [001]. **c** Film lamellae within a tweed-orthoclase lamella (only partly seen) of a mesoperthite (VSL718, $Ab_{48.7}Or_{51.1}An_{0.2}$). The film lamellae are probably twinned after the pericline law (not seen in this section). Electron beam parallel to [001]. **d** Film lamellae with periodic Pericline twinning. As for the Albite twins, the periodicity varies with lamellar width. The orientation of the Pericline twin composition plane is as in analbite or high albite, $\sigma \approx -2°$ (VSL295). Electron beam parallel to [010]

to adopt the shape of spindles. The spindles are more elongated in sections $\parallel(010)$ than they are in sections $\parallel(001)$. We will call such perthites spindle perthites (which is a term found in the German literature; e.g. Voll 1969) (Figs. 2c, 3a). The term film perthite will be used when straight, thin (≤ 1–2 μm) film (albite) lamellae dominate the exsolution texture (Figs. 3, 4). The films are of variable extent, but usually less than ≈ 100 μm. They may or may not be accompanied by similarly thin, but more irregular and much shorter rods (Fig. 3a–c), called fine-scale spindles due to their submicroscopic appearance (Fig. 6a, b). In contrast to the mesoperthitic lamellae and the coarse spindles, films and fine-scale spindles are coherently intergrown with their matrix (see below).

Film and fine-scale spindle exsolution is widespread in Sri Lankan alkali feldspars. It occurs in the Or-rich lamellae of mesoperthites, between lenses and blebs of spindle perthite, and as the only single exsolution texture in Or-rich alkali feldspars. Similar textures were observed by Yund et al. (1980) in granulite-facies feldspars from Finland.

Origin of alkali feldspars

The alkali feldspars of Sri Lanka have formed in one of four different ways:

1. Alkali feldspars crystallized before Pan-African metamorphism from a granite, syenite or pegmatite melt (e.g. Older Metagranites). In these rocks relictic phenocrysts can occasionally be identified from their shapes, sizes, Karlsbad twins and inclusions that have preserved magmatic features. The phenocrysts are found in all stages of deformation, usually they are completely recrystallized. The exsolved plagioclase domains in the non-recrystallized phenocrysts are *not* relics from a stage of cooling and exsolution before deformation and metamorphism: In the northern HC, where the phenocrysts recrystallized after deformation but before cooling, parents and recrystallized grains develop the same exsolution textures after the peak. This requires that the crystals which originally unmixed during magmatic cooling were later homogenized during prograde metamorphism.

2. Alkali feldspars and plagioclases grown from partial melts – produced in several stages of metamorphism – and from pegmatoid sills, crystallized as homogeneous solid solutions. All subsolidus changes are induced by metamorphic cooling.

3. Blasts of alkali feldspar and plagioclase in (psammo-) pelites have grown by prograde mineral reactions. Many of the plagioclase blasts contain trails of quartz, biotite or sillimanite inclusions forming an internal s_1, with or without helizitic rotation. Plagioclase is generally unzoned. The perthites in the (psammo-) pelites have the same exsolution features as the alkali feldspars grown from a melt before the Pan-African metamorphism, which supports the concept that exsolution textures are not pre-Pan-African.

4. Alkali feldspars were deformed and recrystallized at all stages of their development. In the northern HC, the deformed parent crystals were homogeneous solid solutions at peak temperatures, and recrystallized grains forming from them were homogeneous, too. Both exsolved later to form coarse spindle perthites. In the central and southern HC, deformation affected alkali feldspars that were already exsolved (Fig. 3d). In this case, recrystallization divided perthitic grains into separate grains of different orientation which appear as aggregate clusters containing predominantly Or-rich feldspars and little plagioclase. Where a plagioclase parent recrystallized, the aggregate is composed of plagioclase only, and where antiperthite recrystallized, it consists of much plagioclase and little Or-rich feldspar. In Or-rich recrystallizates spindles segregate on further cooling. They are finer than those from the first exsolution event. Such recrystallized and exsolved alkali feldspars may undergo deformation and recrystallization again at lower temperatures. Up to four generations of recrystallized grains have been observed. Of these, the younger generations, which formed at lower temperature, are smaller and exsolve successively finer spindles. The last, Or-rich generation of alkali feldspar recrystallizates segregates film albite and fine-scale spindles only (Fig. 3b).

Experimental methods

After detailed optical inspection of polished thin sections crystals cut approximately parallel to (001) were selected for microprobe work using wavelength dispersive analysis (WDA) and scanning electron microscopy (SEM) on a Cameca microprobe (CAMEBAX MB) and a JEOL Superprobe (JXA-8600MX). Elements Na, K, Ca, Ba, Al, Si, Mg, and Fe were routinely analysed. Operating conditions were: accelerating voltage 15 kV, specimen current 18 nA for the CAMECA and 15 nA for the JEOL instrument. The CAMEBAX data were reduced using the PAP correction of Pouchou and Pichoir (1984), whereas the Bence and Albee (1968) routine was employed for the JEOL Superprobe data.

Point analyses with a focussed beam (≈ 1 µm) were used to obtain phase compositions and a defocussed beam (50 µm–100 µm) to obtain bulk compositions. Depending on the homogeneity of the exsolution pattern, the grains were partly or fully covered by broad spots touching each other. Bohlen and Essene (1977) point out that a matrix-effect error occurs during data correction, because element concentrations vary drastically within a grain, but X-ray intensities are corrected as if the grain were a homogeneous phase. The authors state, however, that these "errors are probably well within experimental error". The film albite lamellae are too thin to be analysed by microprobe. We used TEM energy dispersive analysis (AEM) on one sample (VSL510), the composition of which we think is representative of film albite. The analytical error is larger than in the case of WDA and may amount to ± 3 mol%. All analyses are listed in Table 1.

Small disks (≈ 100 µm–300 µm in diameter) were drilled out of thin sections, using a diamond drilling device mounted on a microscope stage (Medenbach 1986), and used as samples for X-ray single-crystal precession photography of the reciprocal lattice planes a^*b^* and c^*b^*.

For the TEM investigation grains of interest were located in thin sections, cut out and thinned to electron transparency by ion-beam etching. The thinned crystals were studied using a JEM-100C and a Philips 400 TEM, respectively, using bright-field, dark-field and diffraction techniques. High-resolution imaging (ARM) was done with an ARM-1000 at the National Center for Electron Microscopy at the Lawrence Berkeley Laboratory.

Results

Microprobe work

Figure 2a, b are SEM photographs of a coarse mesoperthite (VSL523, bulk composition $Or_{50.3}Ab_{44.9}An_{4.8}$) consisting of (black) Ab-rich and (white) Or-rich lamellae. Within the Or-rich lamellae fine, straight Ab-rich films occur, which sometimes merge into the broad Or-rich lamellae, but sometimes appear to be isolated. We do not know, however, where they terminate in the third dimension. In more Ab-rich mesoperthites with thin Or-rich lamellae, film albite is rare.

At higher bulk Or-content the texture consists of isolated lamellae and elongated lenses (VSL295, bulk composition $Or_{61.0}Ab_{38.5}An_{0.5}$, Fig. 2c). Again, between lamellae and lenses film albite occurs (Fig. 2d). In more Or-rich crystals like VSL510 ($Or_{76.8}Ab_{20.3}An_{2.4}Cn_{0.5}$) few separated blebs are left with abundant films and fine-scale spindles in between (Fig. 3a).

Table 1. Electron microprobe analyses of alkali feldspars from amphibolite and granulite-facies rocks of Sri Lanka

Sample	Mol%	Bulk	L_2	M_2	M_3	L_3
VSL16	Ab	20.9	72.0	17.7	10.2	–
Spindle perthite	Or	77.0	0.8	81.5	88.5	–
	An	1.6	27.2	0.6	0.4	–
	Cn	0.5	0.0	0.2	0.9	–
VSL48–1	Ab	23.1	70.8	19.1	10.0	–
Spindle perthite	Or	72.7	0.8	78.9	88.5	–
	An	3.8	28.5	0.8	0.5	–
	Cn	0.4	0.0	1.2	1.0	–
VSL48–2	Ab	18.3			9.5	–
Alkali feldspar	Or	80.0			89.2	–
recrystallized	An	0.6			0.2	–
from VSL48-1	Cn	1.1			1.1	–
VSL48-3	Ab	72.2				
Plagioclase	Or	1.0				
recrystallized	An	26.8				
from VSL48-1	Cn	0.0				
VSL207	Ab	21.7	74.4	15.7	8.4	–
Spindle perthite	Or	75.7	0.7	82.7	90.1	–
	An	1.4	24.9	0.6	0.2	–
	Cn	1.2	0.0	0.0	1.3	–
VSL295	Ab	38.5	97.6	10.9	8.2	–
Spindle perthite	Or	61.0	0.4	89.1	91.8	–
	An	0.5	2.0	0.0	0.0	–
	Cn	0.0	0.0	0.0	0.0	–
VSL505	Ab	34.6	80.8	15.7	8.5	–
Spindle perthite	Or	61.1	0.7	82.6	89.7	–
	An	3.1	18.5	0.3	0.1	–
	Cn	1.2	0.0	1.4	1.7	–
VSL510	Ab	20.3	62.7	15.3	9.2	88–90
Spindle perthite	Or	76.8	0.8	83.4	89.9	7–8
	An	2.4	36.5	0.6	0.4	3–4
	Cn	0.5	0.0	0.7	0.5	0
VSL522	Ab	23.3	79.8	13.4	9.5	–
Spindle perthite	Or	72.9	0.9	84.8	90.3	–
	An	3.1	19.3	0.3	0.5	–
	Cn	0.7	0.0	1.5	1.7	–
VSL523	Ab	44.9	84.0	16.7	8.7	–
Mesoperthite	Or	50.3	0.9	83.0	91.0	–
	An	4.8	15.1	0.3	0.3	–
	Cn	0.0	0.0	0.0	0.0	–
VSL718	Ab	48.7	98.4	–	6.5	–
Mesoperthite	Or	51.1	1.2	–	93.5	–
	An	0.2	0.4	–	0.0	–
	Cn	0.0	0.0	–	0.0	–
VSL1422	Ab	17.1			6.2	–
Film perthite	Or	81.2			92.0	–
	An	0.6			0.5	–
	Cn	1.1			1.3	–

Note: "bulk" means integrated composition of the alkali feldspar; in case of the spindle perthites, L_2 is the composition of the coarse plagioclase spindles, M_2 is the bulk composition of the Or-rich matrix between the coarse spindles, and M_3 is the composition of the matrix between the film lamellae in areas of M_2 composition. The film lamellae L_3 themselves are too thin to be analysed with the electron microprobe. For VSL510 their composition has been determined by AEM. In case of the mesoperthite, M_2 and L_2 are the compositions of the alkali feldspar and plagioclase lamellae, respectively

If the bulk Or content exceeds ≈80 mol%, only films and fine-scale spindles are exsolved (Fig. 3b, c). Figure 3b (VSL48, $Or_{80.0}Ab_{18.3}An_{0.6}Cn_{1.1}$) shows three grains that intersect at a triple point. Thin sections of the rock sample show that deformed spindle perthites, in response to deformation, partly or completely recrystallized into smaller, undeformed grains (Fig. 3d). Recrystallization separates the Or-rich matrix (VSL48-1, M_2, Table 1) and the Ab-rich plagioclase spindles (L_2) into grains of different orientation, i.e. the parent grains were unmixed,

before they were deformed. The recrystallized grains are dominantly Or-rich alkali feldspar (as in Fig. 3b, d) and subordinate Ab-rich plagioclase. They have virtually the same (bulk) compositions as the matrix and the spindles of the parent grains (compare M_2 and L_2 of VSL48-1 with the bulk compositions of VSL48-2 and 48-3). The Or-rich recrystallizates exsolve film albite later. The film lamellae are less abundant in the interior of the grains to which the fine-scale spindles are restricted (Fig. 3c). In rare cases, these may also be found in the rim. However, in no case do the films occur in the centre with the spindles in the rim. Typically, films only are observed in small grains (Fig. 3d). It is important to note that despite the morphological zonation, observed in Fig. 3b, c, we found from defocussed beam analyses that the recrystallizates are not chemically zoned. The exsolution texture is thus not related to a compositional gradient.

In all the samples the bulk composition M_2 of films and fine-scale spindles plus their Or-rich matrix as well as the composition M_3 of the matrix itself have been determined, avoiding contamination by adjacent lamellae as far as possible. The films and spindles are too thin to be analysed by microprobe. The results are listed in Table 1 together with other samples not described above, but of similar occurrence.

It is seen from Table 1 that the Or content (M_3) of the Or-rich matrix between the film lamellae is very uniform ranging between 88.5 and 91.8 mol% Or. This may indicate a narrow range of closure temperatures for exsolution. The range of compositional variation of lamellae L_2 and matrix M_2 is simply related to the bulk alkali feldspar composition.

Precession photography

In the lower part of Fig. 2c a circular crater is seen. This part of the crystal was drilled out of the thin section for X-ray analysis with a precession camera. Enlarged portions of the photographs with 400 and 060 reflections are shown as inset. The 400 (no. 1) and the 060 (no. 4) reflections represent the Or-rich matrix (Table 1, VSL295-M_3), whereas the merging pair of 400 reflections (no. 2) and the 060 reflection (no. 5) belong to the broad perthitic lamellae (L_2). They constitute a non-coherent intergrowth, which has been documented with the TEM (Evangelakakis 1992). This is consistent with the separation of the two 060 reflections (Smith 1974, Fig. 5.2). Doubling of the 400 reflections is caused by Albite twinning of the Ab-rich phase. The twin periodicity is submicroscopic. The twin reflections are of equal intensity, that is, twinning is balanced. The 400 separation is very small, because the γ^*-angle is close to 90°. The composition of the lamellae is nearly pure albite (Table 1, VSL295-L_2). From the magnitude of the γ^*-angle it follows that the albite is ordered with respect to Al, Si (low albite). Just on top of the 400 pair a very weak single reflection (no. 3) can be seen. It represents the film lamellae, which constitute only a small volume fraction. They are coherently intergrown with the matrix M_3, as demonstrated below by TEM. Due to lattice strain their 0k0 reflections coincide with the matrix reflections, whereas for compensation their a^*-axis is a little longer than in the unstrained low albite lamellae. This results in anomalous cell dimensions, characteristic for coherent intergrowth (e.g. Brown and Willaime 1974; Yund and Tullis 1983). The singularity of the 400 reflection is not proof that the film lamellae are untwinned. In fact TEM imaging reveals twinning at a very fine scale causing weak satellite reflections not seen on the precession photograph (Fig. 4a).

We have prepared single-crystal photographs of areas with film and fine-scale spindle exsolution in a number of crystals representing the whole variety of textures they occur with. We always found them to be coherently intergrown, as demonstrated by similar precession photographs as those shown in Figs. 2c and 3b.

Transmission electron microscopy

The films occur on a microscopic as well as a submicroscopic scale. In TEM micrographs taken on sections ⊥[001] most of the films were found to be Albite twinned (Fig. 4a, b), others were Pericline twinned (Fig. 4c, ⊥[001], Fig. 4d, ⊥[010]). They are embedded in a tweed-orthoclase matrix. The twin periodicity of the films varies with lamellar width, decreasing towards the lamellar tips. Willaime and Gandais (1972) demonstrated that due to coherency stress the twin periodicity is related to the thickness of the exsolution lamellae. Periodicities and thicknesses from Fig. 4 and similar micrographs, plotted in the diagram of Willaime and Gandais (1972), modified by Brown and Parsons (1984), fulfill the expected relationship (Fig. 5).

The position of the rhombic section depends on the lattice parameters of the crystal at the time of twinning. The lattice parameters themselves strongly depend on

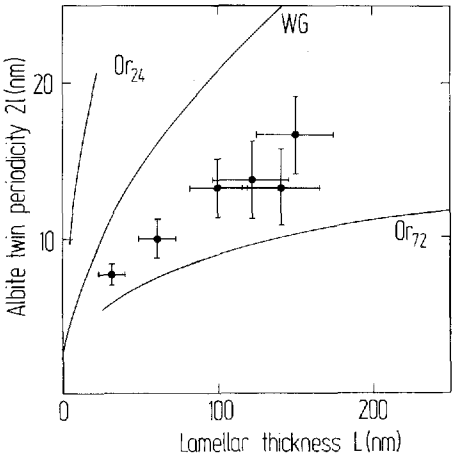

Fig. 5. Variation of the Albite twin periodicity with the thickness of the film lamellae. The error bars represent one standard deviation obtained from the measurement of several film lamellae. *Curve WG*, from Willaime and Gandais (1972), *curves* Or_{24} and Or_{72} from McLaren (1974). Compare with Fig. 2 of Brown and Parsons (1984)

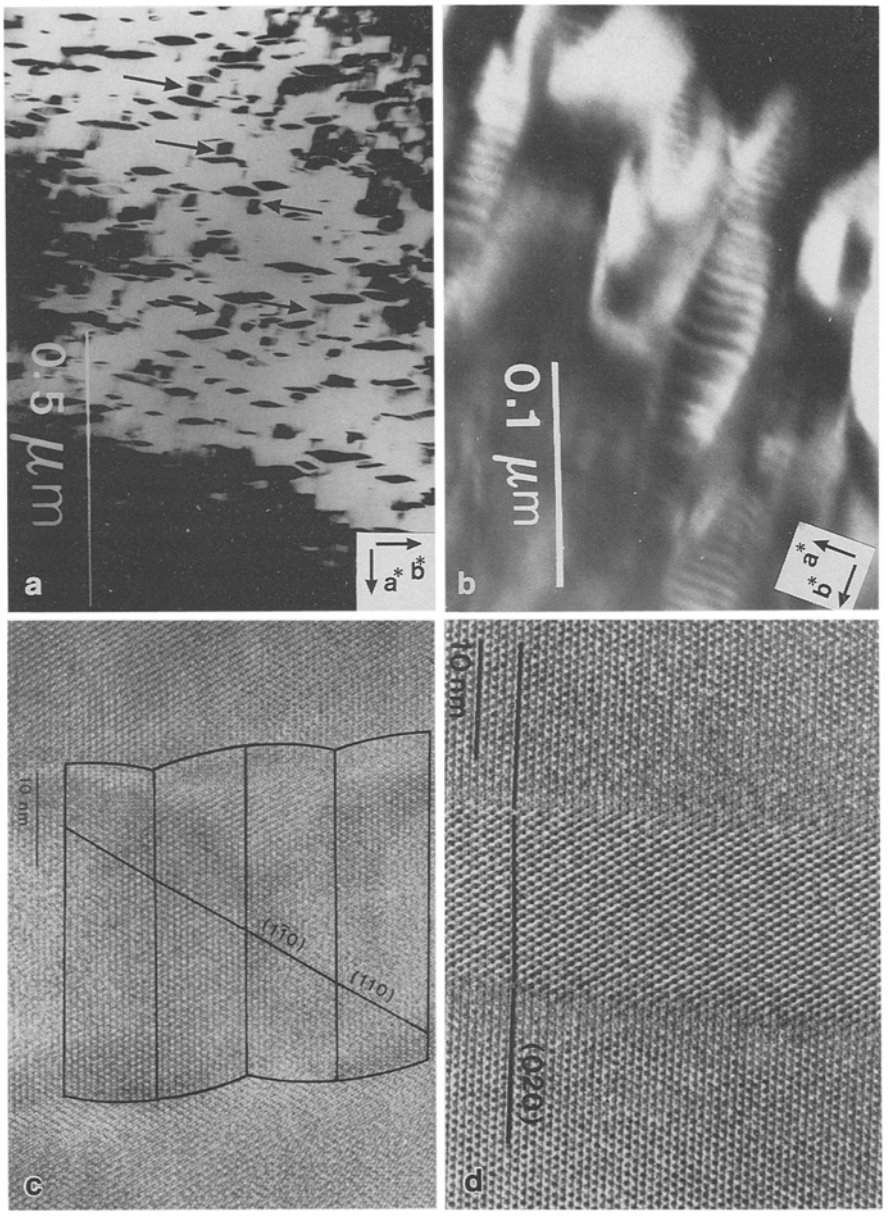

Fig. 6. a Dark-field electron micrograph of an assemblage of fine-scale spindles in VSL48-2. Note rhombic shape of some spindles and their diagonal alignment. *Arrows* point to strain contrast observed between the tips of adjacent spindles. Electron beam parallel to [001]. **b** Dark-field electron micrograph of fine-scale spindles showing periodic Albite twinning (VSL48-2). Electron beam parallel to [001]. **c** Multibeam ARM micrograph of Albite-twinned film albite. The 020, 110 and $1\bar{1}0$ fringes demonstrate coherent intergrowth between film Albite and orthoclase matrix. The 110 and $1\bar{1}0$ fringes bend at the Albite-twin composition planes and at the boundary between film lamella and orthoclase matrix. Note the corrugated interface between matrix and lamella (compare Brown and Parsons 1988). Electron beam parallel to [001]. **d** Multibeam ARM micrograph of a section through a single Pericline twin domain of a film albite. The 020, 110 and $1\bar{1}0$ fringes demonstrate coherent intergrowth between orthoclase matrix and film albite. Electron beam parallel to [001]

the state of the Al,Si order. The micrograph in Fig. 4d is from sample VSL295, a nearly pure alkali feldspar. The film lamellae are virtually free of Ca and poor in K. When combining the electron micrograph with the corresponding a^*c^* diffraction pattern, we find that the angle of the rhombic section is $\sigma \approx -2°$. This is the orientation of the rhombic section in analbite or high albite. The film lamellae thus grew in a highly disordered state.

The structural state, which they possess now, can be estimated from the γ^*-angles measured on a precession photograph. Albite-twinned film lamellae gave apparently monoclinic diffraction patterns (Figs. 2c and 3b) due to the small twin periodicity, whereas in photographs of Pericline-twinned lamellae, in which twinning must have been broader, twin-related spots could be imaged. In the a^*b^*-plane of one of the two Pericline twin sets the γ^*-angle was measured as 88.7°. The composition of a film lamella in sample VSL510 (Table 1) was

determined with an AEM as $Or_{7-8}Ab_{88-90}An_{3-4}$. This composition is thought to be representative of film albite. The limiting γ^*-angles for this composition are 88.3° when the Al,Si distribution is disordered (K,Ca-analbite), and 90.6° when it is ordered (K,Ca-low albite). A γ^*-angle of 88.7° thus indicates a slightly ordered, topochemically triclinic Al,Si distribution as in (K,Ca)-high albite, with $t_1o-t_1m \approx 0.2-0.25$ (Kroll and Ribbe 1987, Fig. 4).

Figure 6a is a micrograph of an assemblage of fine-scale spindles. Some appear to have a rhombic shape with straight edges, and sometimes they tend to be aligned along a diagonal direction which may be related to a minimization of strain energy. Between the tips of some adjacent spindles strain contrast can be noted. Figure 6a to some degreee resembles Fig. 1g of Brown and Parsons (1983), who describe the homogeneous nucleation of platelets in a stranded diffusion profile. Figure 6b shows at a higher magnification that the spindles, as well as the films, are periodically twinned.

The coherency of the interface between film albite and the matrix can be demonstrated directly by atomic resolution imaging (ARM). Figure 6c, d shows multi-beam ARM micrographs taken with the beam parallel to [001]. Figure 6c shows an Albite-twinned film albite embedded in a monoclinic matrix. The 020, 110 and $1\bar{1}0$ fringes extend from the matrix into the lamella without discontinuity. The same is true for the Pericline-twin lamella imaged in Fig. 6d. This figure represents a section parallel to the Pericline composition plane through a single twin lamella from a set of lamellae in a film albite (e.g. Fig. 4d).

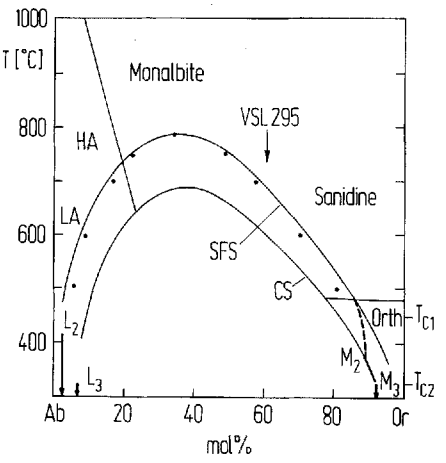

Fig. 7. Behaviour diagram for alkali feldspars of Sri Lankan granulite-facies rocks. *HA*, high albite; *LA*, low albite; *Orth*, tweed-orthoclase; *SFS*, strain-free solvus; *CS*, coherent solvus. The SFS was calculated from Hovis (1991, Eqs. 12–14), the CS was taken from Sipling and Yund (1976). Both were corrected for effects due to changes of pressure (800° C, 8 kbar to 300° C, 3 kbar) and Al,Si order with decreasing temperature. Compositions of the high albite – high sanidine solvus, shown as *dots*, calculated from Hovis are given for comparison. The compositions of the spindles L_2 and their matrix M_2 of the An-poor sample VSL295 are indicated as are the compositions of the film lamellae L_3 (VSL510) and the matrix M_3 between the films (VSL295). During cooling, the compositions of the spindles and their matrix begin to depart from the limbs of the SFS at some temperature $T > T_{c1}$, where T_{c1} is the effective closure temperature for interdiffusion between L_2 and M_2. The cooling path of M_2 intersects the coherent solvus at 400–350° C, where coherent film lamellae L_3 are exsolved. This process continues down to $T_{c2} = 350$–300° C where interdiffusion between L_3 and M_3 ceases

Discussion

Behaviour diagram for alkali feldspars

For better visualization of exsolution processes and corresponding microstructures we illustrate in Fig. 7a behaviour diagram for alkali feldspars. We calculated the strain-free solvus (SFS) for disordered alkali feldspars from Hovis et al. (1991, Eqs. 12–14) assuming, for simplicity, that pressure varied linearly with temperature between 8 kbar, 800°C and 3 kbar, 300° C. The coherent solvus (CS) was taken from Sipling and Yund (1976) and corrected for pressure like the SFS. Both solvi were then adjusted to account for the widening effect of increasing Al,Si order at decreasing temperatures.

The locus of the ordering inversion monalbite-high albite was also corrected for pressure following Ganguly and Saxena (1987, Eq. 4.15'). The value of $\Delta T_c/\Delta P \approx$ 15° C/kbar was estimated from appropriate data by Kroll (1984) and Salje et al. (1985). The monalbite-high albite inversion is second order (Salje et al. 1985), whereas the sanidine-microcline inversion is probably first order with a large step in the order parameter (Kroll and Voll, in Ribbe 1983; Carpenter and Salje 1993). However, because the K-rich feldspars from Sri Lanka are mostly tweed-orthoclase, we approximated the order-disorder transition as continuous.

Cooling paths and compositions of lamellae ($L_{2,3}$) and matrix ($M_{2,3}$) of the samples VSL295 and VSL510 are indicated. They are discussed below.

Temperature of exsolution

The minimum temperature, at which the film lamellae exsolved, can be found from an estimate of the closure temperature T_c for Na,K interdiffusion. Following Dodson (1973, 1986)

$$T_c = \frac{E_a/R}{\ln\left(-\frac{R \cdot A \cdot D_0 \cdot T_c^2}{a^2 \cdot E_a \cdot \mathrm{d}T/\mathrm{d}t}\right)}, \quad (1)$$

where D_0 is the pre-exponential factor and E_a is the activation energy in the Arrhenius equation for diffusion, R is the gas constant, $\mathrm{d}T/\mathrm{d}t$ the cooling rate, A a dimensionless geometrical constant (8.7 for volume diffusion from a plane sheet), and a is a characteristic diffusion distance (e.g. half-width of a plane sheet).

The constants D_0 and E_a in Eq. (1) can be estimated from the temperature dependence of the Na,K interdiffusion coefficient $\bar{D}(X_{Or})$, when the change of $\ln\bar{D}(X_{or})$ with $1/T$ is linearly approximated. We have calculated

$D(X_{Or})$ for $X_{Or}=0.9$ from the relation given by Yund (1984):

$$\bar{D}=\frac{D_K^* \cdot D_{Na}^*}{X_{Or} \cdot D_K^* + (1-X_{Or}) D_K^*}\left[1+\frac{\delta \ln \gamma_{Or}}{\delta \ln X_{Or}}\right], \quad (2)$$

where D_K^* and D_{Na}^* are the K and Na self-diffusion coefficients for a particular composition and γ_{Or} is the activity coefficient in $a_{Or}=\gamma_{Or} \cdot X_{or}$. The first term of Eq. 2 corresponds to the ideal interdiffusion coefficient, the term in square brackets corrects for the non-ideality of the alkali feldspar solid solution. D_K^* and D_{Na}^* of orthoclase Or_{94} were taken from Foland (1974) and extrapolated to lower temperatures. $\ln\gamma_{Or}$ was formulated in terms of Margules parameters as given by Elkins and Grove (1990). For Or-rich compositions the non-ideality term can almost be neglected. At these compositions the term is furthermore virtually identical for strain-free and for coherent alkali feldspars (cf. Brady and Yund 1983).

As demonstrated by Christofferson et al. (1983), D_K^* and D_{Na}^* depend on the diffusion direction. For diffusion parallel to a (about normal to the lamellae) we have calculated $D_o=2.0 \cdot 10^{-3} m^2/s$ and $E_a=288.1$ kJ.

From age dating Hölzl et al. (1991) deduce a cooling rate $-dT/dt=10$–$25°$ C/Ma for the temperature range 600° C to 350–300° C. We will use $dT/dt=-20°$ Ma. Average distances between submicroscopic film lamellae cluster around 0.2 μm (e.g. Fig. 4). From Eq. (1) we find that the closure temperature for Na-K interdiffusion over a distance $a=0.1$ μm is $T_c=318°$ C. A similar estimate was obtained by Yund et al. (1980).

The films and the fine-scale spindles must have nucleated at a somewhat higher temperature in the matrix M_2 (Or_{79-89}). After nucleation the Or content between the exsolving film albite increased to $Or_{>89-92}$ (M_3 measures the composition between the microscopic film lamellae, it thus includes the submicroscopic ones). This composition was reached at T_c. It provides a constraint for the position of the coherent solvus in this temperature range (Fig. 7). This constraint is consistent with the experimentally determined coherent solvus (at 1 bar) for sanidine-high albite (Sipling and Yund 1976), when corrections are made for increased pressure (2–3 kbar at 300–350° C, Schenk et al. 1991) and for increased Al,Si order, considering the low temperature. Pressure and order both increase and widen the solvus.

The maximum temperature for nucleation is given by the position of the matrix composition M_2 on the coherent solvus (Fig. 7). We can only use VSL295 for an estimate, because this is the only sample with no An component in M_2. From Sipling and Yund (1976) we estimate $T \approx 350$–$400°$ C for Or_{89}, when we again allow for increased pressure and order. This maximum temperature of nucleation is well below the stability limit of sanidine ($\approx 480°$ C), so that films nucleated and grew in an orthoclase matrix, the modulated structure of which is seen in Fig. 4a–c. On average, the other samples have 0.5 mol% An in their matrix M_2 which, by comparison with the strain-free ternary solvus, increases the coherent solvus appreciably (say 100–150° C), so that the maximum temperature of nucleation may be roughly 450 to 550° C, but a reliable estimate is difficult to make.

Film perthite: primary or secondary texture?

The question arises whether the film and fine-scale spindle textures represent primary textures or whether they result from an earlier texture. Some pertinent observations follow:

1. From the history of the Sri Lankan rocks we know that no metamorphic and deformational event occurred during or after growth of the films and fine-scale spindles.
2. In all thin sections the appearance of the films is uniform, and in all precession photographs they are seen to be coherently intergrown, that is, they were not subjected to a late hydrothermal event. This would have changed their shape and coherency. In cases where "water" had access to alkali feldspars, we found that: (a) regular exsolution textures give way to patch and band perthite with unbalanced albite twinning of the plagioclase domains; (b) the tweed-texture of orthoclase changes to microcline twinning; (c) swapped rims develop.
3. If the original film perthite texture had been uniform throughout the interior of grains, but with some coarsening along the margins, one would have expected morphological transitions between fine-scale spindles in the centre and film lamellae near the rim. Such a transition has not been observed, however. Furthermore, in large grains of coarse spindle perthite, films and fine-scale spindles both also occur far away from grain boundaries (Figs. 2c, 3a), so that grain boundary interactions as a mechanism of modification seem unlikely.
4. If two adjacent grains are similarly oriented, film lamellae grow from the same site in the common boundary into both grains. This occurs more frequently than would happen by chance or would be produced by modification of an earlier texture (Fig. 3b, d).
5. The same type of texture as in the lower part of Fig. 3b and in Fig. 3d has been produced experimentally by annealing Ge-substituted alkali feldspar between the coherent solvus and the spinode (Kusatz et al. 1987, Fig. 36). This shows that a texture with coherent films nucleating at grain boundaries can be primary.
6. Film perthite is also observed in rocks that have cooled faster than Sri Lankan rocks. It is found in rocks from the Central Swiss Alps, where it may be partly modified by interaction with "water" into irregular and patchy textures. In the Ballachulish aureole, Scotland, small Or-rich alkali feldspar grains occur in quartzites near the contact to the intrusion. They formed by recrystallization from older deformed grains (Kroll et al. 1991). Only the recrystallizates develop film albite. The cooling rate was 20 to 50 times faster than in Sri Lanka: about 500° C/Ma (Buntebarth 1991).

In view of these observations and the low temperatures of film and spindle formation (300–400° C for VSL295) we suggest that the textures are essentially primary with regard to the different morphologies of films

and fine-scale spindles and their mutual distribution in the grains.

Nucleation and exsolution mechanisms

If the textures are in fact primary, we can interpret nucleation and exsolution mechanisms as follows. Film albite preferentially occurs near grain boundaries (Fig. 3b–d), suggesting heterogeneous nucleation. Since the lamellae are coherently intergrown, we conclude that heterogeneous nucleation and coherent intergrowth are not mutually exclusive. In the literature it has sometimes been assumed that heterogeneous nucleation implies incoherency. However, as mentioned above, Kusatz et al. (1987) demonstrated experimentally that below the coherent solvus heterogeneous nucleation may produce coherent intergrowth.

Contrasting to film albite, the fine-scale spindles are concentrated in the centre of the grains, suggesting that they nucleated homogeneously after the films had nucleated but before these had reached the centre of the grains to eliminate the supersaturation of Na. When the grains are small (≈ 100 μm), only films are observed (Fig. 3d), because they arrived at the centre before fine-scale spindles had nucleated. This demonstrates the temperature and time lag between heterogeneous and homogeneous nucleation.

Coherent exsolution does not require breakage of framework bonds. At low temperatures and especially at the dry conditions, which were prevailing in the granulite-facies rocks from Sri Lanka, breaking of Al,Si-O bonds is, kinetically, a very unfavourable process. Coherent exsolution is therefore the only exsolution event in Or-rich alkali feldspars (VSL48-2, VSL1422), and it is the final subsolidus event in the Or-rich matrix (M_2) of coarse meso- and spindle perthites.

Structural state during exsolution and later modifications

The film lamellae and the fine-scale spindles are periodically twinned. The Pericline twins have the same orientation as in analbite or high albite ($\sigma = -2°$). This indicates that the films and spindles grew in a highly disordered state and afterwards twinned. As shown for VSL295, nucleation occurred at $T < 400°$ C, i.e. in the stability field of low albite. Films and spindles to some degree inherited their Al,Si disorder from the overall monoclinic matrix due to the coherent nature of intergrowth. After exsolution, the Al,Si order is not expected to advance appreciably at $T < 400°$C and dry conditions. In fact, the γ^*-angle of 88.7° measured in a precession photograph of Pericline-twinned lamellae still indicates high albite, the rhombic section of which would be $\sigma = +3°$ (calculated from $\gamma = 89.8°$ and $\alpha^* = 88.0°$ corresponding to $t_1o - t_1m = 0.2$–0.25 in pure Na-feldspar). The slight increase in order reflected in the change of σ was probably induced by the increase in triclinicity after twinning.

Parsons and Brown (1991) argued that in ordered feldspars coarsening of a periodically twinned coherent lamella would not only involve Na-K interdiffusion, but would also require an adjustment of the Al,Si distribution which strongly inhibits lateral growth, especially at dry conditions and low temperatures. To a lesser extent their argument also applies to the situation described, where film lamellae with slightly ordered and anti-ordered twin domains are coherently intergrown with the overall monoclinic matrix.

Summary

We summarize the results as follows:

1. Exsolution of film lamellae and fine-scale spindles is nearly omnipresent in the amphibolite- and granulite-facies alkali feldspars of Sri Lanka.
2. Films and spindles were exsolved below the coherent solvus at minimum temperatures of 350 to 300° C and maximum temperatures of about 450 to 550° C. Coherent exsolution avoids breaking of (Al,Si)-O bonds which is a kinetically unfavourable process, especially at low temperatures and dry conditions.
3. The fine-scale spindles presumably nucleated homogeneously, the film lamellae nucleated heterogeneously. Heterogeneous nucleation and coherent growth are not mutually exclusive.
4. The fine-scale spindles are periodically twinned after the Albite law, the films after the Albite and Pericline laws. The composition plane of the Pericline law is the same as in analbite or high albite. The films thus grew at low temperatures in a metastable disordered state and then became periodically twinned. The relation between the twin periodicity and the thickness of the films and fine-scale spindles follows the prediction by Willaime and Gandais (1972) for coherent intergrowth.
5. After twinning, the Al,Si order only slightly increased. The low temperature of exsolution did not allow the films and spindles to attain full order. As a result, high albite is preserved metastably in coherent intergrowth with tweed-orthoclase.
6. If the bulk Or content of the alkali feldspar is less than ≈ 80 mol%, exsolution of films and spindles is preceded at a higher temperature by an exsolution process that produced coarse mesoperthites and spindle perthites. At bulk compositions of $Or_{>80}$ films and fine-scale spindles represent the only exsolution.
7. The exsolution features, i.e. shape and coherency of films and fine-scale spindles, suggest that no late-stage hydrothermal event was effective. The rocks cooled under essentially dry conditions.

Acknowledgement. This work was supported by the Deutsche Forschungsgemeinschaft in the Priority Programme "Stoffbestand, Struktur und Entwicklung der Unterkruste", which is gratefully acknowledged. The manuscript benefited much from thorough reviews by W.L. Brown, Nancy, and R.A. Yund, Providence. We thank G. von Cölln for carefully typing the manuscript and C. Middendorf for the photographic work. We are appreciative for access to facilities at the National Center for Electron Microscopy at the Lawrence Berkeley Laboratory. H.R.W. acknowledges support through NSF grant EAR 9104605.

References

Bence AE, Albee AL (1968) Empirical correction factors for the electron microanalysis of silicates and oxides. J Geol 76:382–403

Bohlen SR, Essene EJ (1977) Feldspar and oxide thermometry of granulites in the Adirondack Highlands. Contrib Mineral Petrol 62:153–169

Brady JB, Yund RA (1983) Interdiffusion of K and Na in alkali feldspars: homogenization experiments. Am Mineral 68:106–111

Brown WL, Parsons I (1983) Nucleation on perthite-perthite boundaries and exsolution mechanisms in alkali feldspars. Phys Chem Miner 10:55–61

Brown WL, Parsons I (1984) The nature of potassium feldspar, exsolution microtextures and development of dislocations as a function of composition in perthitic alkali feldspars. Contrib Mineral Petrol 86:335–341

Brown WL, Willaime C (1974) An explanation of exsolution orientations and residual strain in cryptoperthites. In: MacKenzie WS, Zussman J (eds) The feldspars. Manchester Univ Press, pp 440–459

Buntebarth G (1991) Thermal models of cooling. In: Voll G, Töpel J, Pattison DRM, Seifert F (eds) Equilibrium and kinetics in contact metamorphism. Springer, Berlin Heidelberg New York, pp 267–473

Büsch W, Mehnert KR (1991) Antiperthites in granulites and similar structures in migmatites of the Black Forest. Neues Jahrb Mineral Abh 162:117–133

Cahn JW (1962) Coherent fluctuations and nucleation in isotropic solids. Acta Crystallogr 10:907–913

Cahn JW (1968) Spinodal decomposition. Trans Metall Soc AIME 242:166–180

Carpenter MA, Salje E (1993) Thermodynamics of non-convergent cation ordering in minerals. III. Order parameter coupling in K-feldspar. Am Mineral (in press)

Christofferson RG, Yund RA, Tullis J (1983) Inter-diffusion of K and Na in alkali feldspars: diffusion couple experiments. Am Mineral 68:1126–1133

Day HW, Brown VM (1980) Evolution of perthite compositions and microstructure during progressive metamorphism of hypersolvus granite, Rhode Island, USA. Contrib Mineral Petrol 72:353–365

Dodson MH (1973) Closure temperature in cooling geochronological and petrological systems. Contrib Mineral Petrol 40:259–274

Dodson MH (1986) Closure profiles in cooling systems. Mater Sci For 7:145–154

Elkins LT, Grove TL (1990) Ternary feldspar experiments and thermodynamic models. Am Mineral 75:544–559

Evangelakakis C (1992) Die Entmischungs- und Umwandlungsgefüge der granulitfaziellen Feldspäte Sri Lankas – lichtmikroskopische und elektronenmikroskopische, röntgenographische und mikroanalytische Untersuchungen. PhD thesis, Westfälische Wilhelms-Universität Münster, Germany

Foland KA (1974) Alkali diffusion in orthoclase. In: Hofmann AW, Gilett BJ, Yoder HS Jr, Yund RA (eds) Geochemical transport and kinetics. Carnegie Inst Washington Academic Press, New York, pp 77–98

Fuhrman ML, Lindsley DH (1988) Ternary-feldspar modeling and thermometry. Am Mineral 73:201–215

Ganguly J, Saxena SK (1987) Mixtures and mineral reactions. Springer, Berlin Heidelberg New York

Geological Map of Sri Lanka, 8 miles to one inch (1982) Geol Surv Dep, Colombo, Sri Lanka

Hölzl S, Köhler H, Kröner A, Jaeckel P, Liew TC (1991) Geochronology of the Sri Lankan basement. In: Kröner A (ed) The crystalline crust of Sri Lanka. I. Summary of research of the German-Sri Lankan Consortium. Geol Surv Dep of Sri Lanka, Prof Pap 5:237–257

Hovis GL, Delbove F, Bose MR (1991) Gibbs energies and entropies of K-Na mixing for alkali feldspars from phase equilibrium data: implications for feldspar solvi and short-range order. Am Mineral 76:913–927

Kay SM (1977) The origin of antiperthites in anorthosites. Am Mineral 62:905–912

Kleinschrodt R (1993) Large scale thrusting in the lower crustal basement of Sri Lanka. Precambrian Res (in press)

Kleinschrodt R, Voll G, Kehelpannala W (1991) A layered basic intrusion, deformed and metamorphosed in granulite facies of the Sri Lanka basement. Geol Rundsch 80:779–800

Kroll H (1984) Thermal expansion of alkali feldspars. In: Brown WL (ed) Feldspars and Feldspathoids. Reidel Publ Co, Dordrecht, pp 163–205

Kroll H, Ribbe PH (1987) Determining (Al,Si) distribution and strain in alkali feldspars using lattice parameters and diffraction-peak positions: a review. Am Mineral 72:491–506

Kroll H, Krause C, Voll G (1991) Disordering, re-ordering and unmixing in alkali feldspars from contact-metamorphosed quartzites. In: Voll G, Töpel J, Pattison DRM, Seifert F (eds) Equilibrium and kinetics in contact metamorphism. Springer, Berlin Heidelberg New York, pp 267–473

Kroll H, Evangelakakis C, Voll G (1993) Two-feldspar geothermometry: a review and revision for slowly cooled rocks. Contrib Mineral Petrol 114:510–518

Kusatz B, Kroll H, Kaiping A, Pentinghaus H (1987) Mechanismus und Kinetik von Entmischungsvorgängen am Beispiel Ge-substituierter Alkalifeldspäte. Fortschr Mineral 65:203–248

McLaren AC (1974) Transmission electron microscopy of the feldspars. In: McKenzie WS, Zussman J (ed) The feldspars. Manchester Univ. Press, Manchester, pp 378–423

Medenbach O (1986) Ein modifiziertes Kristallbohrgerät nach Verschure (1978) zur Isolierung kleiner Einkristalle aus Dünnschliffen. Fortschr Mineral 64 Beihe 1:113

Mora CI, Valley JW (1985) Ternary feldspar thermometry in granulites from the Oaxacan Complex, Mexico. Contrib Mineral Petrol 89:215–225

Parsons I (1978) Feldspars and fluids in cooling plutons. Mineral Mag 42:1–17

Parsons I, Brown WL (1984) Feldspars and the thermal history of igneous rocks. In: Brown WL (ed) Feldspars and feldspathoids, D Reidel Publ Co, Dordrecht, pp 317–371

Parsons I, Brown WL (1991) Mechanisms and kinetics of exsolution – structural control of diffusion and phase transformations in alkali feldspars. In: Ganguly J (ed) Diffusion, atomic ordering, and mass transport. (Advances in physical geochemistry, vol 8) Springer, Berlin Heidelberg New York, pp 304–344

Pouchou J-L, Pichoir F (1984) A new model for quantitative X-ray microanalysis. Rech Aerosp 3:13–38

Raith M, Faulhaber S, Hoffbauer R, Spiering B (1991) Characterization of high-grade metamorphism in the southern part of Sri Lanka. In: Kröner A (ed) The crystalline crust of Sri Lanka. I. Summary of research of the German-Sri Lankan Consortium. Geol Surv Dep of Sri Lanka, Prof Pap 5, pp 164–177

Ribbe PH (1983) Aluminum-silicon order in feldspars: domain textures and diffraction patterns. In: Ribbe PH (ed) Feldspar Mineralogy. (Reviews in mineralogy, 2, 2nd edn) Mineral Soc Am, Washington DC, pp 21–55

Salje E, Kuscholke B, Kroll H (1985) Thermodynamics of sodium feldspar. II. Experimental results and numerical calculations. Phys Chem Miner 12:99–107

Schenk V, Raase P, Schumacher R (1991) Metamorphic zonation and P–T history of the highland complex in Sri Lanka. In: Kröner A (ed) The crystalline crust of Sri Lanka. I. Summary of research of the German-Sri Lankan Consortium. Geol Surv Dep of Sri Lanka, Prof Pap 5:150–163

Schumacher R, Faulhaber S (1993) Evaluation of P–T estimates on garnet-pyroxene-plagioclase-quartz bearing granulite-facies rocks from Sri Lanka. Precambrian Res (in press)

Schumacher R, Schenk V, Raase P, Vitanage PW (1990) Granulite facies metamorphism of metabasic and intermediate rocks in

the Highland Series of Sri Lanka. In: Ashworth JR, Brown M (eds) High-grade metamorphism and crustal anatexis. Allen and Unwin, London, pp 235–271

Sipling PJ, Yund RA (1976) Experimental determination of the coherent solvus for sanidine-high albite. Am Mineral 61:897–906

Smith JV (1974) Feldspar minerals. I. Crystal structure and physical properties. Springer, Berlin Heidelberg New York

Smith JV, Brown WL (1988) Feldspar minerals, vol 1, 2nd edn. Springer Verlag, Berlin Heidelberg New York

Speer JA, Ribbe PH (1973) The feldspars of the Kiglapait intrusion, Labrador. Am J Sci 273A:468–478

Voll G (1969) Klastische Mineralien aus den Sedimentserien der Schottischen "Highlands" und ihr Schicksal bei aufsteigender Regional- und Kontaktmetamorphose. Habilitation thesis, Berlin

Voll G, Kleinschrodt R (1991) Sri Lanka: structural, magmatic and metamorphic development of a Gondwana fragment. In: Kröner A (ed) The crystalline crust of Sri Lanka. I. Summary of research of the German-Sri Lankan Consortium. Geol Surv Dep of Sri Lanka, Prof Pap 5, pp 22–51

Voll G, Evangelakakis C, Kroll H (1993) Revised two-feldspar geothermometry applied to Sri Lankan feldspars. Precambrian Res (in press)

Willaime C, Gandais M (1972) Study of exsolution in alkali feldspars calculation of elastic stresses inducing periodic twins. Phys Status Solidi 9:529–539

Worden RH, Walker FDL, Parsons I, Brown WL (1990) Development of microporosity, diffusion channels and deuteric coarsening in perthitic alkali feldspars. Contrib Mineral Petrol 104:507–515

Yund RA (1983a) Microstructure, kinetics and mechanisms of alkali feldspar exsolution. In: Ribbe PH (ed) Feldspar mineralogy. (Reviews in mineralogy, vol 2, 2nd edn) Mineral Soc Am, Washington DC, pp 177–202

Yund RA (1983b) Diffusion in feldspars. In: Ribbe PH (ed) Feldspar mineralogy. (Reviews in mineralogy, vol 2, 2nd edn) Mineral Soc Am, Washington DC, pp 203–239

Yund RA (1984) Alkali feldspar exsolution: kinetics and dependence on alkali interdiffusion. In: Brown WL (ed) Feldspars and feldspathoids, D Reidel Publ Co, Dordrecht, pp 281–315

Yund RA, Ackermand D (1979) Development of perthite and microstructures in the Storm King Granite, N.Y. Contrib Mineral Petrol 70:273–280

Yund RA, Tullis J (1983) Strained cell parameters for coherent lamellae in alkali feldspars and iron-free pyroxenes. Neues Jahrb Miner Monatsh 1:22–34

Yund RA, Ackermand D, Seifert F (1980) Microstructures in the alkali feldspars from the granulite complex of Finnish Lapland. Neues Jahrb Mineral Monatsh 3:109–117

Editorial responsibility: J. Hoefs